Sensors & Actuators: B. Chemical 280 (2019) 94–101

Contents lists available at ScienceDirect

Sensors and Actuators B: Chemical

journal homepage: www.elsevier.com/locate/snb

Lysosome-targeting NIR ratiometric luminecent upcoversion nanoprobe toward arginine

Zhanxian Li[a,b], Hanxiao Liu[a], Haixia Li[a], Yung-Hao Tsou[b], Yilin Gao[c], Xiaoyang Xu[b,**], Weiwei Du[a], Liuhe Wei[a], Mingming Yu[a,b,*]

[a] College of Chemistry and Molecular Engineering, Zhengzhou University, Zhengzhou, 450001, China
[b] Department of Chemical and Materials Engineering, New Jersey Institute of Technology, Newark, NJ, 07102, USA
[c] Department of Chemistry, State Key Laboratory of Molecular Engineering of Polymers, Institutes of Biomedical Sciences & Collaborative Innovation Center of Chemistry for Energy Materials, Fudan University, 220 Handan Road, Shanghai, 200433, PR China

ARTICLE INFO

Keywords:
Upcoversion
Nanoprobe
Lumine
Scence
Arginine
LRET

ABSTRACT

Near-infrared (NIR) fluorescent sensors have been actively pursued due to organisms exhibiting little autofluorescence in near-infrared regions. Capable of emitting luminesence under 980 nm excitation, upconversion nanoparticles have shown promise as optical agents for in vivo bioimaging. Based on luminescence resonance energy transfer (LRET), a NIR luminescent Arg-nanoprobe was developed by the decoration of upconversion nanoparticles (UCNPs) ($NaYF_4$:Yb,Er) with organic molecules. The as-developed nanoprobe could quantitatively detect concentrations within the range of 528–1250 μM, and had high sensitiviy (the limit of detection, LOD, being 15.6 μM) and good photostability. Because the probe could target lysosomes, intracellar detection of Arg behavior was demonstrated via upconversion luminescence (UCL) imaging.

1. Introduction

For quite a long time, Arg has attracted the attention of scientists due to its indispensability to the human body. Arg is responsible for protein synthesis and the production of many substances. Moreover, Arg has an important role in many life activities, such as wound healing, cell division, and hormone release [1,2]. Therefore, it is crucial to develop an effective method for selective and sensitive recognition of Arg.

Fluorescent molecular probes have extensive applications in numerous fields, such as disease diagnosis and environmental detection [3–8]. As a result, many organic molecular probes have been developed for examining metal ions [9–13], anions [14–17], pH [18–21], and biological molecules [22–27]. Although Arg is significant for humans, only a few molecular probes have been developed for its recognition [28–31].

Ratiometric detection has been regarded as a way to overcome the interference effects of instrumental parameters, photobleaching, the microenvironment around the probe molecule, etc. [32–34]. LRET, which has been considered to be a satisfactory luminescence recognition mode, has been widely adopted in ratiometric detection [35,36]. Up to now, very few LRET-based ratiometric luminescent probes for Arg have been reported and thus it is very significant to design LRET-based Arg probes.

Currently, Arg probes excited with UV–vis light are most reported [28–30]. A hopeful strategy for the design of luminescent Arg-nanoprobes is the use of upconversion nanoparticles, which exhibit upconversion luminescence when excited with NIR light, as well as outstanding light penetration depth in tissues, and can eliminate spontaneous fluorescence from biological samples [37–39]. At 980 nm excitation, the upconversion nanoparticles (UCNPs) were applied as LRET donors; the organic dyes, as LRET acceptors [40–42].

UCNPs-1 is the first upconversion luminescence (UCL) probe developed for ratiometric bioimaging of Arg. Fig. 1a illustrates the mechanisms involved in Arg sensing. With this UCNPs-organic molecule architecture, the probe demonstrates several merits. First, its excitation at 980 nm makes it capable of offering greater depth of penetration in tissues. Second, as a LRET-based Arg probe, it can provide more accurate detection in biosystem and improve signal-to-noise ratios. Third, it displays good photostability, selectivity, and anti-interference ability. Lastly, due to its lysosome-targeting ability, the ratiometric probe allows accurate intracellular tracking of Arg.

* Corresponding author at: College of Chemistry and Molecular Engineering, Zhengzhou University, Zhengzhou, 450001, China.
** Corresponding author.
E-mail addresses: xiaoyang.xu@njit.edu (X. Xu), yumm@zzu.edu.cn (M. Yu).

https://doi.org/10.1016/j.snb.2018.10.057
Received 9 April 2018; Received in revised form 9 October 2018; Accepted 9 October 2018
Available online 10 October 2018

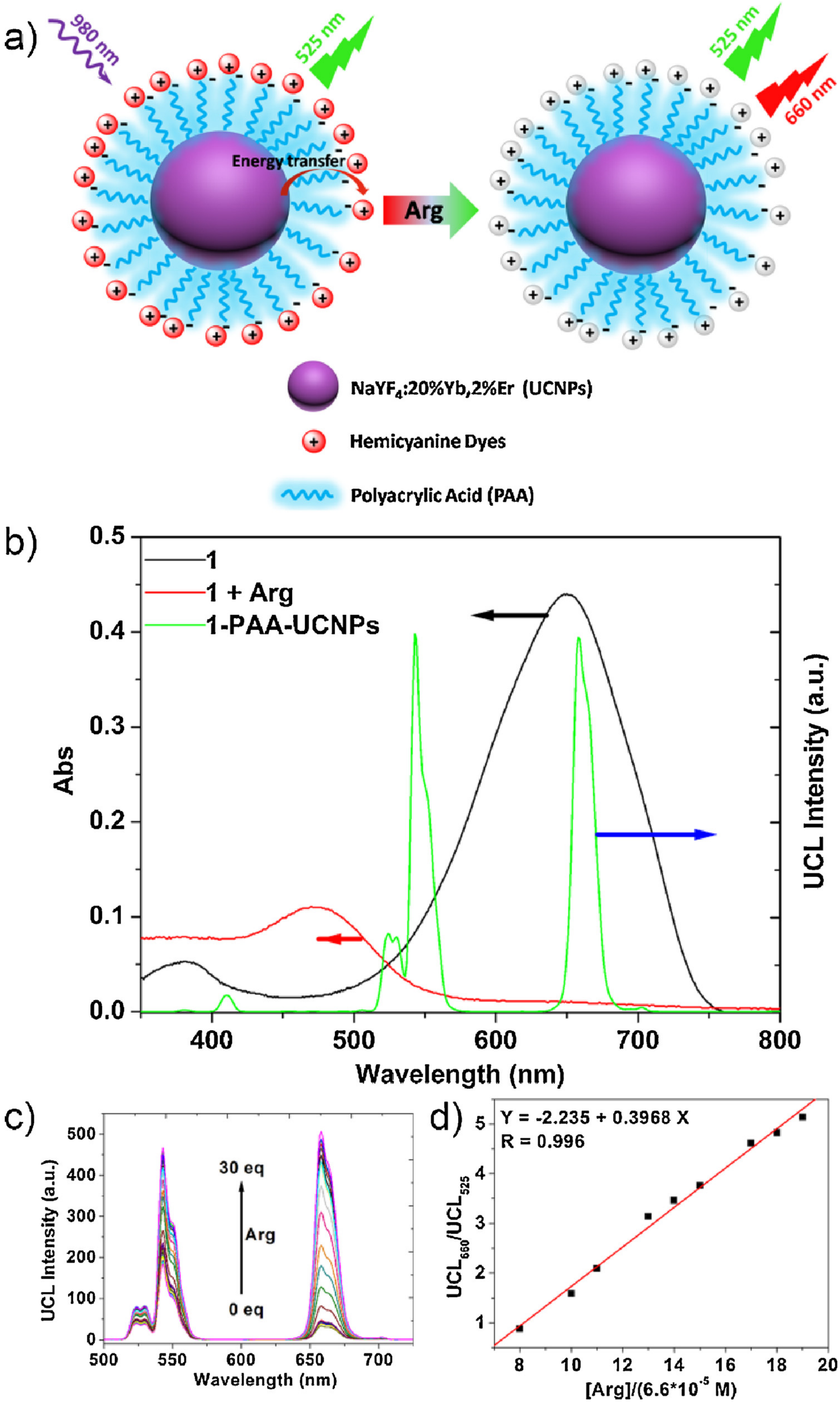

Fig. 1. (a) Schematic illustration of the LRET-based ratiometric nanoprobe for Arg synthesized from hemicyanine dye-modified UCNPs (not to scale). (b) Absorption spectra of probe **1** (1.0×10^{-5} M) in 8:2 (v/v) water/DMSO solution (black and red lines) and luminescence spectrum of UCNPs (0.50 mg/mL) under 980 nm excitation in water (green line). (c) Upconversion emission spectra of **UCNPs-1** (0.50 mg/mL) under 980 nm excitation in 8:2 (v/v) water/DMSO solution upon titration of Arg water solution. (0 eq or 30 eq is Arg concentration to the concentration of the loading compound **1** in **UCNPs-1** particle.) (d) The linearity of emission intensity ratio of UCL_{660}/UCL_{525} to increasing Arg concentration. The numbers on X-axis represent Arg concentration to the concentration of the loading compound **1** in **UCNPs-1** particle (For interpretation of the references to colour in this figure legend, the reader is referred to the web version of this article).

2. Experimental

2.1. Materials and methods

Iodomethane, *p*-hydrazinobenzoic acid hydrochloride, 3-amino phenol, K_2CO_3, dimethylacetone, 1,4-dibromobutane, Pd-C catalyst, ethyl pyruvate, SeO_2, 1,4-dioxane, DMF AcOH, AcONa, 4-Hydroxybenzaldehyde, alanine (Ala), isoleucine (Ile), methonine (Met), threonine (Thr), tryptophane (Trp), cysteine (Cys), homocysteine (Hcy), glucose (Glc), H_2O_2, NaCl, $MgCl_2$, KCl, $CaCl_2$, $MnCl_2$, $CoCl_2$, $ZnCl_2$, Na_2SO_3, NaHS, $NaClO_3$, NaF, $Na_2C_2O_4$, $NaHSO_3$, $Na_2S_2O_3$, NaI, Na_2SO_4, $NaNO_3$, $NaClO_4$, $NaHCO_3$, Na_2HPO_4 NaAc, NaBr, Na_3N,

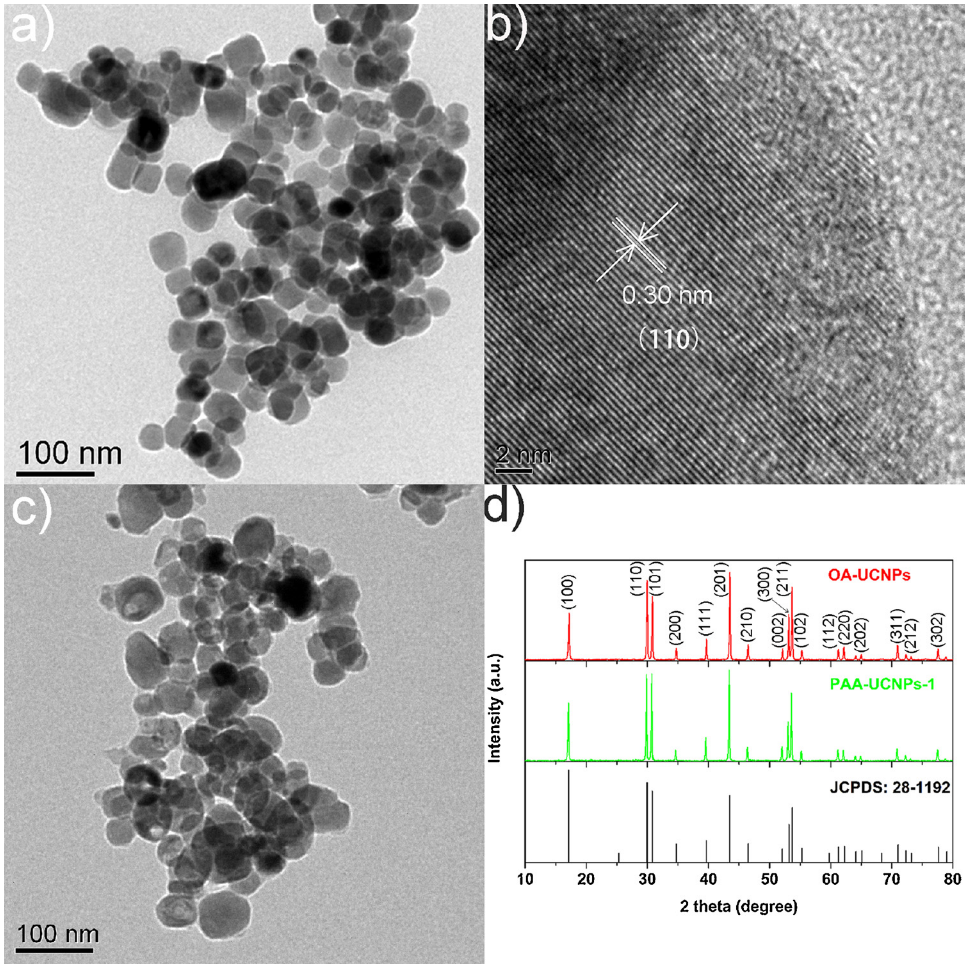

Fig. 2. (a) TEM image of $NaYF_4$:Yb,Er nanoparticles. (b) Typical HRTEM image of as-prepared $NaYF_4$:Yb,Er nanoparticles. (c) TEM image of PAA modified $NaYF_4$:Yb,Er nanoparticles. (d) XRD patterns of OA modified $NaYF_4$:Yb,Er and PAA modified $NaYF_4$:Yb,Er nanoparticles.

NaH_2PO_4, $C_{17}H_{35}COOH$, polyacrylic acid (PAA, Mw = 1800), Y_2O_3, Yb_2O_3, and Er_2O_3 were used directly unless otherwise specified.

Mass spectra were measured on a Tesla FTMS-MALDI/DHB mass spectrometer. Nuclear magnetic resonance (NMR) spectra were obtained on a Bruker (400 MHz) instrument. Low-resolution TEM were measured on a JEOL-JEM 2100 transmission electron microscopy operated at 200 kV. High resolution TEM was carried out on a JEOL-JEM 2100 F field emission transmission electron microscope. XRD patterns were determined on a Rigaku D/MAX-2000 diffractometer.

2.2. Synthesis of rare earth stearate precursor

Y_2O_3 (880.7 mg, 3.9 mmol), Yb_2O_3 (394.1 mg, 1.0 mmol) and Er_2O_3 (38.3 mg, 0.1 mmol) were added to 20 mL concentrated nitric acid and heated to volatilize excessive nitric acid. The rare earth nitrate was obtained as white powder, in which the mole ratio of Y^{3+}, Yb^{3+}, and Er^{3+} was 0.78:0.20:0.02. The mixture of 80 mL ethanol solution of the above salts and 8.5344 g (30 mmol) stearic acid were gradually heated to 78 °C and refluxed, and then 20 mL ethanol solution of NaOH (1.1900 g, 30 mmol) was titrated and refluxed for 1 h. The mixture was filtrated, and the filter cake was washed with twice water and once with ethanol. The stearic acid precursor was gained after drying the filter cake for 12 h in vacuum drying box.

2.3. Synthesis of $NaYF_4$:Yb,Er [43]

The as-prepared stearate precursor (957.7 mg, 1.0 mmol) and NaF (209.9 mg, 5 mmol) were added to 15 mL ethanol, 5 mL OA, and 10 mL H_2O. The reaction solution was stirred for 15 min and then transferred to a hydrothermal synthesis reactor. After reacting for 1 d at 150 °C, the mixture was cooled. The mixture of $CHCl_3$ and EtOH (v/v = 1:6) was added to the precipitate and the crude product was obtained after centrifugal separation as white powder. After washing thrice with water-ethanol (v/v = 1:2) and once with ethanol, the white powder was dispersed in $CHCl_3$.

2.4. Preparation of PAA modified upconversion nanoparticles [44,45]

The saturated dichloromethane solution of $NOBF_4$ was titrated to 30 mL $CHCl_3$ colloidal solution of hydrophobic $NaYF_4$:Yb,Er nanoparticles and the mixture was stirred for 15 min. By centrifugal separation, the precipitate was washed with ethanol and dissolved in DMF. After precipitated in tolune, the precipitate was collected by filtration and dissolved in DMF. 300 mg PAA was added slowly to the above DMF solution and then 60 mL acetone was added. After stirring for 12 h, centrifugation (18,000 rpm, 15 min), and washing with water, the PAA-modified nanoparticles were collected and redispersed in water.

2.5. Preparation of **UCNPs-1** [46]

For the preparation of upconversion nanoparticles, a mixture of compound **1** (45.72 mg) in DMSO and UCNPs (5 mg/mL) in 20 mL water was stirred for 12 h. After centrifuging, the resulting precipitate

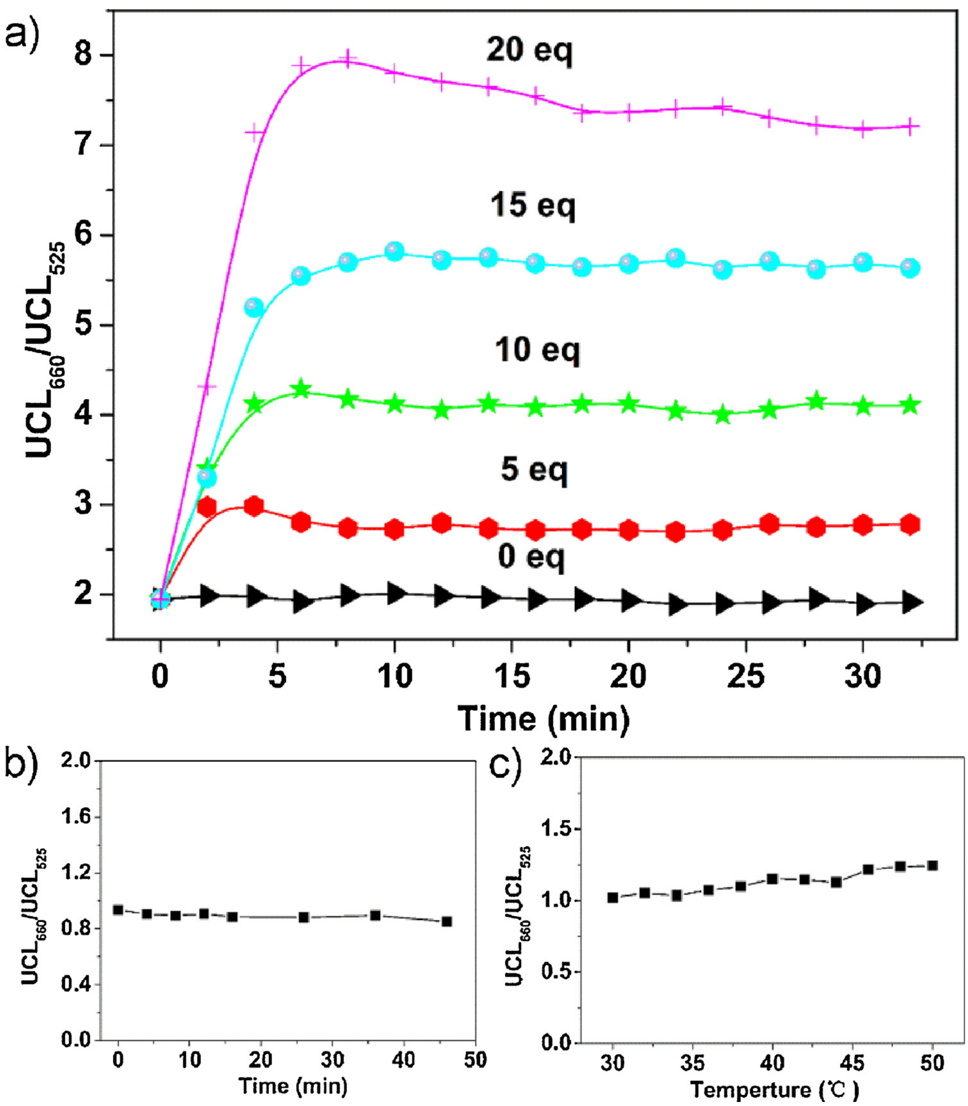

Fig. 3. (a) Kinetic curves of probe **UCNPs-1** [0.50 mg/mL in 8:2 (v/v) water/DMSO] at 660 nm and 525 nm with Arg at different concentrations (the concentrations of Arg are 0 (black line), 3.3×10^{-4} M (red line), 6.6×10^{-4} M (green line), 9.9×10^{-4} M (blue line), 1.3×10^{-3} M (cyan line). The excitation wavelength was 980 nm. (b) UCL ratio (UCL_{660}/UCL_{525}) of 0.50 mg/mL **UCNPs-1** in water–DMSO solution (8:2, v/v) as irradiation (λ_{ex} = 980 nm) time changes. (c) UCL ratio (UCL_{660}/UCL_{525}) of 0.50 mg/mL **UCNPs-1** in water–DMSO solution (8:2, v/v) as temperature changes (For interpretation of the references to colour in this figure legend, the reader is referred to the web version of this article).

was collected and washed three times with water. After heating the as-prepared solid at 60 °C in vacuum drying box, the nanocomposite material (**UCNPs-1**) was obtained.

2.6. Detection of Arg in solution phase

All the detection experiments were carried out in 8:2 (v/v) water/DMSO solution, the concentration of compound **1** was 6.6×10^{-6} M and the amount of compound **1** in the hybrid material was 7.51% its weight. UV–vis absorption spectra were obtained with a TU-1901 spectrophotometer. Photoluminescence (PL) and PL excitation spectra were measured on a Hitachi F-4600 spectrometer with 980 nm pump laser source.

2.7. Cell viability

Cell viability was determined with 3-(4,5-dimethylthiazol-2-yl) -2,5-diphenyltetrazolium bromide (MTT) assay. HeLa cells were seeded into 96-well plates at a density of 5×10^3 cells per well in DMEM (10% FBS) in six replicates and incubated for 24 h. After that the cells were exposed to 0, 8.3, 13.6, 27.3, 54.5, and 109.1 μg/mL **UCNPs-1** for 1 h, then medium was discard and replaced with 100 μL fresh medium for 24 h, then 10 μL MTT (5 mg/mL) was added, and the cells were further incubated for 5 h at 37 °C. The medium was removed and the formazan crystals were dissolved in DMSO. The absorbance at 570 nm and the background value at 690 nm were measured with enzyme labelling instrument, and then the cell survival rate was calculated.

2.8. Detection of Arg in cells

The HeLa cells were incubated with 6 μg/mL **UCNPs-1** for fluorescence imaging. The fluorescent images were recorded with 660 nm filters after the cells incubated with probe **UCNPs-1** (6 μg/mL, 37 °C) for 30 min. After adding 2.0×10^{-5} M and 2.8×10^{-5} M Arg respectively and incubation for 30 min, the fluorescent images were taken at the same situation. The excitation was performed at 980 nm.

3. Results and discussion

To fabricate the recognition system, organic compound was synthesized as the recognition part and energy acceptor. The synthetic routes are shown in Scheme S1. The synthetic details and characterization data can be found in our previous work [47,48].

The peaks at 650 and 475 nm, respectively, represented the maximum absorption of **1** without and with Arg in 8:2 (v/v) water/DMSO solution. The main emission peaks of UCNPs (0.50 mg/mL) were located approximately at 525, 575 and 660 nm in water solution (excited at 980 nm, Fig. 1b). The significant spectral overlap of NIR excitation source and the absorption of **1** indicated LRET between Yb^{3+}–Er^{3+} pairs and **1**. Hence, the NIR 980 nm excitation source can be selected to

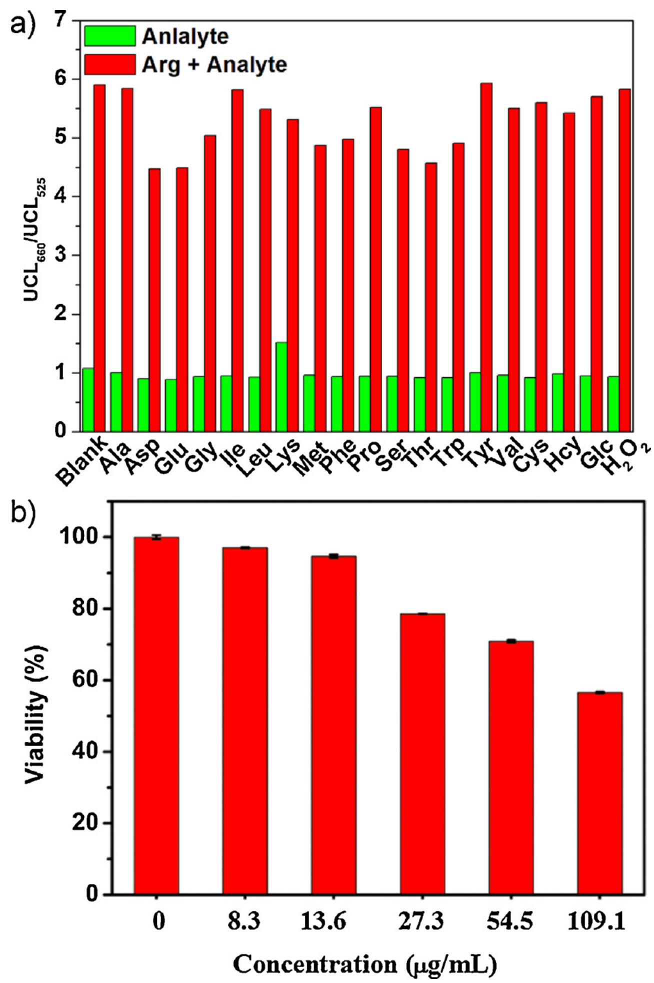

Fig. 4. (a) UCL responses of **UCNPs-1** [0.50 mg/mL in 8:2 (v/v) water/DMSO] under 980 nm excitation upon addition of different species (2.0×10^{-3} M) (green bars) and UCL responses of the mixture of **UCNPs-1** and Arg (2.0×10^{-3} M in water) under 980 nm excitation after addition of an excess of the indicated species (2.0×10^{-3} M) (red bars). The reaction time was 40 min. UCL_{660} and UCL_{525} represent the UCL intensity at 660 nm and 525 nm. The species used were Ala, Asp, Glu, Gly, Ile, Leu, Lys, Met, Phe, Pro, Ser, Thr, Trp, Tyr, Val, Cys, Hcy, Glc, and H_2O_2. (b) Viability assay for HeLa cells treated with probe **UCNPs-1** in dark (For interpretation of the references to colour in this figure legend, the reader is referred to the web version of this article).

excite UCNPs. The luminescence of UCNPs was absorbed by compound **1** completely. After the addition of Arg, an emission band centered at 660 nm was recovered. The absorbance of compound **1** at 525 nm was almost the same with or without Arg. That is to say, the emission at 525 nm hardly changes whether **1** is with or without Arg.

Based on the absorption spectra of **UCNPs-1** in the solution (the 4th line of Fig. S2), the concentration of the loading compound **1** could be determined (6.6×10^{-6} M) (Fig. S2 in Supporting information). In the following experiments, the concentration of compound **1** was 6.6×10^{-6} M and the amount of compound **1** in the hybrid material was 7.51% its weight.

Figures S3 and S4 (Supporting information) present the absorption spectral response of **1** and upconversion emission spectral change of PAA-UCNPs upon titration of Arg water solution. It is clear that the absorbance of **1** at 650 nm decreased dramatically as Arg concentration increased (Fig. S3). Arg induced the decomposition of compound **1** (Fig. 1b) [48]. The upconversion lumincence (UCL) spectrum hardly changed upon addition of Arg (Fig. S4). Considering Figs. 1b, S3 and S4, it is easy to conclude that the addition of Arg can lead to the absorption spectral conversion of compound **1** and does not impact the UCL spectra.

An aqueous solution (containing 20% DMSO) was utilized as the medium to determine the luminescence spectral change of **UCNPs-1** at different Arg concentrations. As shown in Fig. 1c, when the Arg concentration increased from 0 to 2.0×10^{-3} M and the **UCNPs-1** were excited at 980 nm, the peak centered at 660 nm increased gradually and the peak centered at 525 nm shifted little in intensity. The changes in the upconversion spectrum can be ascribed to the Arg-induced decomposition of compound **1** and LRET between the energy donor (UCNPs) and the energy acceptor (compound **1**). In Fig. 1d, a good linear relationship between UCL_{660}/UCL_{525} and Arg concentration, varying from 525 μM to 1250 μM, was observed. The linear calibration was shown in Fig. 1d, and the detection limit of the probe **UCNPs-1** was 15.6 μM according to the signal-to-noise ratio [49,50], thus showing that **UCNPs-1** makes an excellent ratiometric Arg UCL probe.

Although the UCNPs were developed with a ligand exchange process [51–53], the $NaYF_4$:Yb,Er particles were produced using a previously reported procedure [54,55]. The TEM image (Fig. 2a) reveals that the particles had a diameter ranging between 21 and 63 nm (Fig. S7). The HRTEM photographs show a distinct lattice distance of 0.30 nm, matching the (110) plane of hexagonal phase $NaYF_4$:Yb,Er nanoparticles (Fig. 2b). The TEM image of PAA-UCNPs (Fig. 2c) indicates that there was a layer of organic membrane outside the nanoparticles, implying that PAA was successfully coated on the surface of the nanoparticles. Fig. 2d demonstrates the XRD patterns of as-prepared lanthanide-doped upconversion nanoparticles (The patterns of OA-UCNPs and **1-PAA-UCNP**s coincide with each other.), which were identified with the standard pattern (JCPDS 28–1192) and indicate that surface modification does not change the crystal phase of the nanoparticles. In the FTIR spectra (Fig. S1 in Supporting information), the peaks at 1578, 1622, and 1722 cm^{-1} are corresponding compound **1**.

The kinetic curves (Fig. 3a) showed that the reaction between UCNPs-1 and Arg completely finished within 5 min at which the Arg concentration was 6.6×10^{-4} M. In the photostability experiment, the luminescence intensity ratio of UCL_{660} to UCL_{525} (UCL_{660}/UCL_{525}) did not shift with irradiation time (Fig. 3b), indicating excellent photostability. Whereas, for the thermal stability experiment, in which the temperature was increased from 30 to 48 °C, the UCL ratio shifted slightly, indicating good thermal stability. It can therefore be concluded that the **UCNPs-1** as an Arg probe has excellent photostability and better thermal stability.

Various species, including nucleophilic biological molecules (Pro, Tyr, Val, Ser, Glu, Gly, Met, Trp, Lys, Thr, Phe, Ala, Asp, IIe, Leu, Cys, Hcy, Glc, and H_2O_2), metal ions (Mn^{2+}, K^+, Ca^{2+}, Na^+, Zn^{2+}, Co^{2+}, and Mg^{2+}) and anions (F^-, Cl^-, Br^-, I^-, N_3^-, NO_3^-, ClO_3^{2-}, ClO_4^-, $C_2O_4^{2-}$, SH^-, $S_2O_3^{2-}$, SO_3^{2-}, HSO_3^{2-}, SO_4^{2-} and HPO_4^{2-}), were investigated (Figs. 4a, S5 and S6). UCL responses upon addition of different species revealed that **UCNPs-1** as a ratiometric Arg-probe has good selectivity. Interference experiments toward the various above mentioned species indicate that the **UCNPs-1** had strong anti-interference ability (Figs. 4a, S5 and S6 in Supporting information). The cytotoxicity experiments were carried out to extend further application of probe UCNPs-1. HeLa cells were incubated with probe UCNPs-1 at different concentrations 0, 8.3, 13.6, 27.3, 54.5 and 109.1 μg/mL for 24 h. As shown in Fig. 4b, HeLa cells did not show obvious influence and the cell viability was still more than 90% even under the incubation of 13.6 μg/mL probe for as long as 24 h. These results suggested that probe UCNPs-1 has low cytotoxicity and good biocompatibility to the cultured cells and can be used to image Arg in living cells.

UCNPs-1 was applied to image intracellular Arg-targeting lysosomes. The cells stained with 6 μg/mL **UCNPs-1** (5 h, 25 °C) were further co-stained with a commercially available lysosome-specific dye Neutral Red (2.0 mM, 30 min). The pictures indicate that the red image acquired upon 980 nm was almost exactly same as the purple one gained upon excitation at 543 nm (Fig. 5). These results suggest that **UCNPs-1** has the ability to target lysosomes ascribing to the tertiary

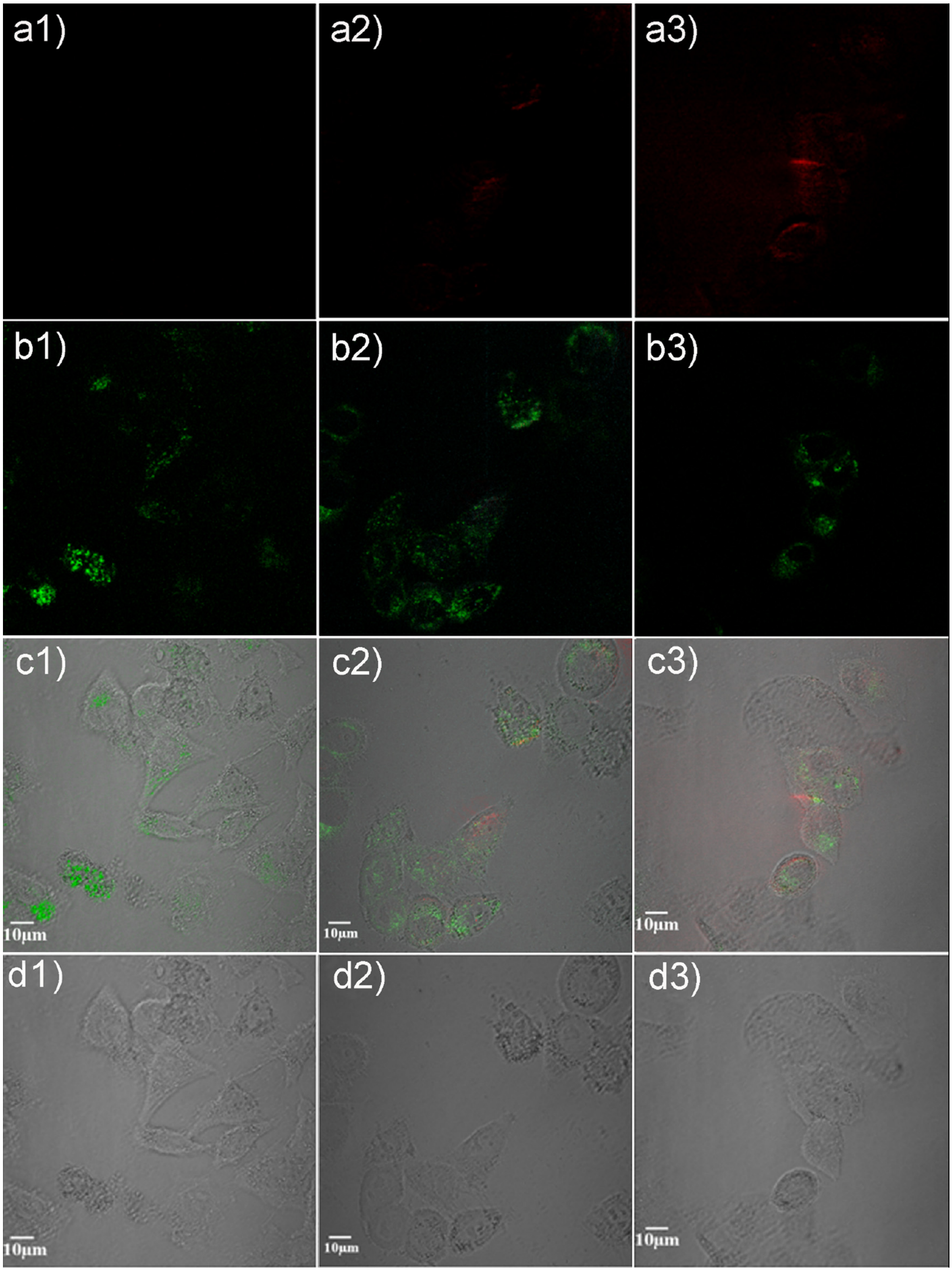

Fig. 5. Confocal UCL images of Hela cells stained with 6 μg/mL **UCNPs-1** for 5 h (Channel 1: λ_{ex} = 980 nm, λ_{em} = 660 nm) and different concentrations of Arg ((a1) 0, (a2) 2.0×10^{-5} M, and (a3) 2.8×10^{-5} M). Confocal fluorescence images of Hela cells stained with Lysosome-Tracker red (2.0 mM) for 30 min (Channel 2: λ_{ex} = 543 nm, λ_{em} = 590 nm) and different concentrations of Arg ((b1) 0, (b2) 2.0×10^{-5} M, and (b3) 2.8×10^{-5} M). Merged images of (a) and (b) (c1, c2 and c3). Bright field images of (a), (b) and (c) (d1, d2 and d3) (For interpretation of the references to colour in this figure legend, the reader is referred to the web version of this article).

amino group of compound **1** [48,56].

The confocal UCL microscopy cellular imaging experiments of HeLa cells after incubation with **UCNPs-1** upon 980 nm excitation are shown in Fig. 5. **UCNPs-1** nanoparticles were incubated with HeLa cells for 5 h at 37 °C. Luminescence was not detected at the red channel, verifying excellent cell permeability. After subsequent addition of different concentrations of Arg (2.0×10^{-5} M and 2.8×10^{-5} M), an obvious gradual increase of luminescence at the red channel was recorded. The cells before and after treatment with Arg did not change throughout bright-field imaging experiments.

4. Conclusion

In summary, a LRET-based NIR ratiometric UCL Arg nanoprobe was developed. The NIR LRET-based ratiometric nanoprobe for Arg displayed excellent photostability, good selectivity, strong anti-interference ability, low cytotoxicity, and lysosome-targeting abilities. Overall, this research may provide a new approach for constructing NIR ratiometric Arg probes of improved accuracy.

Acknowledgements

We are grateful for the financialsupports from National Natural Science Foundation of China (U1704161, U1504203, 21601158), and Zhengzhou University (32210431).

Appendix A. Supplementary data

Supplementary material related to this article can be found, in the online version, at doi:https://doi.org/10.1016/j.snb.2018.10.057.

References

[1] Y. Nonnenmacher, K. Hiller, Biochemistry of proinflammatory macrophage activation, Cell. Mol. Life Sci. (2018) 1–17.

[2] J. Yin, W. Ren, X. Huang, T. Li, Y. Yin, Protein restriction and cancer, Biochim. Biophys. Acta Rev. Cancer 1869 (2018) 256–262.

[3] G.G. Dias, A. King, F. de Moliner, M. Vendrell, E.N. da Silva Júnior, Quinone-based fluorophores for imaging biological processes, Chem. Soc. Rev. 47 (2018) 12–27.

[4] K.G. Chernov, T.A. Redchuk, E.S. Omelina, V.V. Verkhusha, Near-infrared fluorescent proteins, biosensors, and optogenetic tools engineered from phytochromes, Chem. Rev. 117 (2017) 6423–6446.

[5] Y. Ding, W.-H. Zhu, Y. Xie, Development of ion chemosensors based on porphyrin analogues, Chem. Rev. 117 (2017) 2203–2256.

[6] J.-N. Liu, W. Bu, J. Shi, Chemical design and synthesis of functionalized probes for imaging and treating tumor hypoxia, Chem. Rev. 117 (2017) 6160–6224.

[7] D. Wu, A.C. Sedgwick, T. Gunnlaugsson, E.U. Akkaya, J. Yoon, T.D. James, Fluorescent chemosensors: the past, present and future, Chem. Soc. Rev. 46 (2017) 7105–7123.

[8] R.A. Potyrailo, Toward high value sensing: monolayer-protected metal nanoparticles in multivariable gas and vapor sensors, Chem. Soc. Rev. 46 (2017) 5311–5346.

[9] X. Sun, S.D. Dahlhauser, E.V. Anslyn, New autoinductive cascade for the optical sensing of fluoride: application in the detection of phosphoryl fluoride nerve agents, J. Am. Chem. Soc. 139 (2017) 4635–4638.

[10] G. Song, R. Sun, J. Du, M. Chen, Y. Tian, A highly selective, colorimetric, and environment-sensitive optical potassium ion sensor, Chem. Commun. 53 (2017) 5602–5605.

[11] L. Liang, F. Lan, S. Ge, J. Yu, N. Ren, M. Yan, Metal-enhanced ratiometric fluorescence/naked eye bimodal biosensor for lead ions analysis with bifunctional nanocomposite probes, Anal. Chem. 89 (2017) 3597–3605.

[12] L. Li, Y. Fan, Q. Li, R. Sheng, H. Si, J. Fang, L. Tong, B. Tang, Simultaneous single-cell analysis of Na^+, K^+, Ca^{2+}, and Mg^{2+} in neuron-like PC-12 cells in a microfluidic system, Anal. Chem. 89 (2017) 4559–4565.

[13] W. Xu, Z. Zeng, J.H. Jiang, Y.T. Chang, L. Yuan, Discerning the chemistry in individual organelles with small-molecule fluorescent probes, Angew. Chem., Int. Ed. 55 (2016) 13658–13699.

[14] R.Q. Li, Z.Q. Mao, L. Rong, N. Wu, Q. Lei, J.Y. Zhu, L. Zhuang, X.Z. Zhang, Z.H. Liu, A two-photon fluorescent probe for exogenous and endogenous superoxide anion imaging in vitro and in vivo, Biosens. Bioelectron. 87 (2017) 73–80.

[15] R. Kaushik, A. Ghosh, D.A. Jose, Recent progress in hydrogen sulphide (H2S) sensors by metal displacement approach, Coord. Chem. Rev. 347 (2017) 141–157.

[16] S.J. Li, C.Y. Li, Y.F. Li, J. Fei, P. Wu, B. Yang, J.O. Yang, S.X. Nie, Facile and sensitive near-infrared fluorescence probe for the detection of endogenous alkaline phosphatase activity in vivo, Anal. Chem. 89 (2017) 6854–6860.

[17] K. Dou, Q. Fu, G. Chen, F. Yu, Y. Liu, Z. Cao, G. Li, X. Zhao, L. Xia, L. Chen, H. Wang, A novel dual-ratiometric-response fluorescent probe for SO_2/ClO^- detection in cells and in vivo and its application in exploring the dichotomous role of SO_2^- under the ClO^- induced oxidative stress, Biomaterials 133 (2017) 82–93.

[18] C.G. Dai, J.L. Wang, Y.L. Fu, H.P. Zhou, Q.H. Song, Selective and real-time detection of nitric oxide by a two-photon fluorescent probe in live cells and tissue slices, Anal. Chem. 89 (2017) 10511–10519.

[19] A. Wallabregue, D. Moreau, P. Sherin, P.M. Lorente, Z. Jarolimova, E. Bakker, E. Vauthey, J. Gruenberg, J. Lacour, Selective imaging of late endosomes with a pH-sensitive diazaoxatriangulene fluorescent probe, J. Am. Chem. Soc. 138 (2016) 1752–1755.

[20] S.L. Pan, K. Li, L.L. Li, M.Y. Li, L. Shi, Y.H. Liu, X.Q. Yu, A reaction-based ratiometric fluorescent sensor for the detection of Hg (ii) ions in both cells and bacteria, Chem. Commun. 54 (2018) 4955–4958.

[21] X. Chen, K.A. Lee, X. Ren, J.C. Ryu, G. Kim, J.H. Ryu, W.J. Lee, J. Yoon, Synthesis of a highly HOCl-selective fluorescent probe and its use for imaging HOCl in cells and organisms, Nat. protoc. 11 (2016) 1219–1228.

[22] Y. Yue, F. Huo, P. Ning, Y. Zhang, J. Chao, X. Meng, C. Yin, Dual-site fluorescent probe for visualizing the metabolism of Cys in living cells, J. Am. Chem. Soc. 139 (2017) 3181–3185.

[23] X. Han, X. Song, F. Yu, L. Chen, A ratiometric near-infrared fluorescent probe for quantification and evaluation of selenocysteine-protective effects in acute inflammation, Adv. Funct. Mater. 27 (2017) 1700769.

[24] Z. Jarolimova, M. Vishe, J. Lacour, E. Bakker, Potassium ion-selective fluorescent and pH independent nanosensors based on functionalized polyether macrocycles, Chem. Sci. 7 (2016) 525–533.

[25] Z.R. Liu, Y. Tang, A. Xu, W. Lin, A new fluorescent probe with a large turn-on signal for imaging nitroreductase in tumor cells and tissues by two-photon microscopy, Biosens. Bioelectron. 89 (2017) 853–858.

[26] K. Gu, Y. Xu, H. Li, Z. Guo, S. Zhu, S. Zhu, P. Shi, T.D. James, H. Tian, W.H. Zhu, Real-time tracking and in vivo visualization of β-galactosidase activity in colorectal tumor with a ratiometric near-infrared fluorescent probe, J. Am. Chem. Soc. 138 (2016) 5334–5340.

[27] Y. Li, W. Liu, P. Zhang, H. Zhang, J. Wu, J. Ge, P. Wang, A fluorescent probe for the efficient discrimination of Cys, Hcy and GSH based on differentcascade reactions, Biosens. Bioelectron. 90 (2017) 117–124.

[28] W. Lu, Y. Gao, Y. Jiao, S. Shuang, C. Li, C. Dong, Carbon nano-dots as a fluorescent and colorimetric dual-readout probe for the detection of arginine and Cu^{2+} and its logic gate operation, Nanoscale 9 (2017) 11545–11552.

[29] T. Liu, N. Li, J.X. Dong, Y. Zhang, Y.Z. Fan, S.M. Lin, H.Q. Luo, N.B. Li, A colorimetric and fluorometric dual-signal sensor for arginine detection by inhibiting the growth of gold nanoparticles/carbon quantum dots composite, Biosens. Bioelectron. 87 (2017) 772–778.

[30] J.H. Cao, L.P. Ding, W.T. Hu, X.L. Chen, X. Chen, Y. Fang, Ternary system based on fluorophore–surfactant assemblies Cu^{2+} for highly sensitive and selective detection of arginine in aqueous solution, Langmuir 30 (2014) 15364–15372.

[31] X. Zhou, X.J. Jin, D.H. Li, X. Wu, Selective detection of zwitterionic arginine with a new Zn(II)-terpyridine complex: potential application in protein labeling and determination, Chem. Commun. 47 (2011) 3921–3923.

[32] L. Wu, I.C. Wu, C.C. DuFort, M.A. Carlson, X. Wu, L. Chen, C.T. Kuo, Y. Qin, J. Yu, S.R. Hingorani, D.T. Chiu, Photostable ratiometric pdot probe for in vitro and in vivo imaging of hypochlorous acid, J. Am. Chem. Soc. 139 (2017) 6911–6918.

[33] N. Makukhin, V. Tretyachenko, J. Moskovitz, J. Míšek, A ratiometric fluorescent probe for imaging of the activity of methionine sulfoxide reductase a in cells, Angew. Chem. 128 (2016) 12919–12922.

[34] A.T. Aron, M.O. Loehr, J. Bogena, C.J. Chang, An endoperoxide reactivity-based FRET probe for ratiometric fluorescence imaging of labile iron pools in living cells, J. Am. Chem. Soc. 138 (2016) 14338–14346.

[35] J. Zhang, Y. Fu, H.H. Han, Y. Zang, J. Li, X.P. He, B.L. Feringa, H. Tian, Remote light-controlled intracellular target recognition by photochromic fluorescent glycoprobes, Nat. Commun. 8 (2017) 987–996.

[36] X. Jia, Q. Chen, Y. Yang, Y. Tang, R. Wang, Y. Xu, W. Zhu, X. Qian, FRET-based mito-specific fluorescent probe for ratiometric detection and imaging of endogenous peroxynitrite: dyad of Cy3 and Cy5, J. Am. Chem. Soc. 138 (2016) 10778–10781.

[37] X. Wang, R.R. Valiev, T.Y. Ohulchanskyy, H. Ågren, C. Yang, G. Chen, Dye-sensitized lanthanide-doped upconversion nanoparticles, Chem. Soc. Rev. 46 (2017) 4150–4167.

[38] X. Qin, X. Liu, W. Huang, M. Bettinelli, X. Liu, Lanthanide-activated phosphors based on 4f-5d optical transitions: theoretical and experimental aspects, Chem. Rev. 117 (2017) 4488–4527.

[39] Y.S.S. Yang, P.U. Atukorale, K.D. Moynihan, A. Bekdemir, K. Rakhra, L. Tang, F. Stellacci, D.J. Irvine, High-throughput quantitation of inorganic nanoparticle biodistribution at the single-cell level using mass cytometry, Nat. Commun. 8 (2017) 14069–14078.

[40] Y. Liu, S. Zhou, Z. Zhuo, R. Li, Z. Chen, M. Hong, X. Chen, In vitro upconverting/downshifting luminescent detection of tumor markers based on Eu^{3+}-activated core–shell–shell lanthanide nanoprobes, Chem. Sci. 7 (2016) 5013–5019.

[41] Z. Li, T. Liang, S. Lv, Q. Zhuang, Z. Liu, A rationally designed upconversion nanoprobe for in vivo detection of hydroxyl radical, J. Am. Chem. Soc. 137 (2015) 11179–11185.

[42] H. Dong, L.D. Sun, C.H. Yan, Energy transfer in lanthanide upconversion studies for extended optical applications, Chem. Soc. Rev. 44 (2015) 1608–1634.

[43] M. Wang, J.L. Liu, Y.X. Zhang, W. Hou, X.L. Wu, S.K. Xu, Two-phase solvothermal synthesis of rare-earth doped $NaYF_4$, upconversion fluorescent nanocrystals, Mater. Lett. 63 (2009) 325–327.

[44] A. Dong, X. Ye, J. Chen, Y. Kang, T. Gordon, J.M. Kikkawa, C.B. Murray, A generalized ligand-exchange strategy enabling sequential surface functionalization of colloidal nanocrystals, J. Am. Chem. Soc. 133 (2011) 998–1006.

[45] X.Y. Zheng, L.D. Sun, T. Zheng, H. Dong, Y. Li, Y.F. Wang, C.H. Yan, PAA-capped GdF_3 nanoplates as dual-mode MRI and CT contrast agents, Chin. Sci. Bull. 60 (2015) 1092–1100.

[46] J. Peng, W. Xu, C.L. Teoh, S. Han, B. Kim, A. Samanta, J.C. Er, L. Wang, L. Yuan, X.G. Liu, Y.T. Chang, High-efficiency in vitro and in vivo detection of Zn^{2+} by dye-assembled upconversion nanoparticles, J. Am. Chem. Soc. 137 (2015) 2336–2342.

[47] B. Shi, Y. Gao, C. Liu, W. Feng, Z. Li, L. Wei, M. Yu, A ratiometric fluorescent sensor for pH fluctuation and its application in living cells with low dark toxicity, Dyes Pigments 136 (2017) 522–528.

[48] M. Yu, W. Du, H. Li, H. Zhang, Z. Li, Near-infrared ratiometric fluorescent detection of arginine in lysosome with a new hemicyanine derivative, Biosens. Bioelectron. 92 (2017) 385–389.

[49] D.H. Yu, F.H. Huang, S.S. Ding, G.Q. Feng, Near-infrared fluorescent probe for detection of thiophenols in water samples and living cells, Anal. Chem. 86 (2014) 8835–8841.
[50] M.M. Yu, W.W. Du, W. Zhou, H.X. Li, C.X. Liu, L.H. Wei, Z.X. Li, H.Y. Zhang, A 1,8-naphthalimide-based chemosensor with an off-on fluorescence and lifetime imaging response for intracellular Cr^{3+} and further for S^{2-}, Dyes Pigm. 126 (2016) 279–285.
[51] P. Lei, R. An, S. Yao, Q. Wang, L. Dong, X. Xu, K. Du, J. Feng, H. Zhang, Ultrafast synthesis of novel hexagonal phase $NaBiF_4$ upconversion nanoparticles at room temperature, Adv. Mater. 29 (2017) 1700505.
[52] J.C. Boyer, F. Vetrone, L.A. Cuccia, J.A. Capobianco, Synthesis of colloidal upconverting $NaYF_4$ nanocrystals doped with Er^{3+}, Yb^{3+} and Tm^{3+}, Yb^{3+} via thermal decomposition of lanthanide trifluoroacetate precursors, J. Am. Chem. Soc. 128 (2006) 7444–7445.
[53] H.X. Mai, Y.W. Zhang, R. Si, Z.G. Yan, L.D. Sun, L.P. You, C.H. Yan, High-quality sodium rare-earth fluoride nanocrystals: controlled synthesis and optical properties, J. Am. Chem. Soc. 128 (2006) 6426–6436.
[54] R. Wei, Z. Wei, L. Sun, JinZ. Zhang, J. Liu, X. Ge, L. Shi, Nile red derivative-modified nanostructure for upconversion luminescence sensing and intracellular detection of Fe^{3+} and MR imaging, ACS Appl. Mater. Interfaces 8 (2016) 400–410.
[55] Z.W. Wei, L.N. Sun, J.L. Liu, J.Z. Zhang, H.R. Yang, Y. Yang, L.Y. Shi, Cysteine modified rare-earth up-converting nanoparticles for in vitro and in vivo bioimaging, Biomaterials 35 (2014) 387–392.
[56] G. Li, D. Zhu, L. Xue, H. Jiang, Quinoline-based fluorescent probe for ratiometric detection of lysosomal pH, Org. Lett. 15 (2013) 5020–5023.